Comparison of the Ferromagnetic Phase Transitions in La0.7Ca0.3MnO3 and Single Crystal Nickel by Micromagnetic Imaging

James Loudon, P A Midgley

Comparison of the Ferromagnetic Phase Transitions in $La_{0.7}Ca_{0.3}MnO_3$ and Single Crystal Nickel by Micromagnetic Imaging

Journal:	*Philosophical Magazine & Philosophical Magazine Letters*
Manuscript ID:	TPHM-05-Sep-0408.R1
Journal Selection:	Philosophical Magazine
Date Submitted by the Author:	14-Nov-2005
Complete List of Authors:	Loudon, James; University of Cambridge, Department of Materials Science and Metallury Midgley, P; University of Cambridge, Department of Materials Science and Metallurgy
Keywords:	transmission electron microscopy, electron holography, ferromagnetism, manganites, nickel, phase transitions
Keywords (user supplied):	

Comparison of the Ferromagnetic Phase Transitions in $La_{0.7}Ca_{0.3}MnO_3$ and Single Crystal Nickel by Micromagnetic Imaging

J. C. LOUDON* and P. A. MIDGLEY

Department of Materials Science and Metallurgy, University of Cambridge, Pembroke Street, Cambridge, CB2 3QZ, UK

There is considerable controversy surrounding the nature of the paramagnetic to ferromagnetic phase transition in $La_{0.7}Ca_{0.3}MnO_3$. We have used transmission electron microscopy to perform micromagnetic imaging in order to determine whether the phase change is first or second order. On warming through the transition point, the ferromagnetic phase retreats from the sample surface as it is replaced by the paramagnetic phase. This coexistence of ferromagnetic and paramagnetic phases indicates a primarily first order transition. However, there is also a continuous loss of magnetisation which precedes the phase transition. We compare this with the ferromagnetic transition in nickel which displays a purely continuous phase change. We discuss the accuracy and range of applicability of the micromagnetic imaging techniques of electron holography and Fresnel imaging which were used in this investigation.

Keywords: manganite; micromagnetic; electron microscopy; Fresnel; electron holography; ferromagnet; phase transition; nickel.

1. Introduction

At first sight, distinguishing between first and second order phase transitions appears deceptively simple: at the transition point of a first order phase transition, two different phases are present whereas a second order transition takes place in a continuous manner and only one phase is present at a given temperature [1]. In thermodynamic experiments, it is usual to distinguish between different orders of phase transition by heating the sample at a known rate and measuring the temperature increase. If heat can be supplied with no corresponding increase in temperature, this is the latent heat needed to grow a new phase within the old phase and the transition is first order. Other tests involve looking for signs of metastable phases near the transition point since the formation of metastable phases is only possible in a first order transition. Thus if the sample behaves differently during warming and cooling experiments (thermal hysteresis), the transition is first order. Finally, one can look for discontinuities in quantities related to the first derivative of the Gibbs' free energy (such as magnetisation or thermal expansion coefficient) since these are only found in a first order transition. If any of these tests yield a positive result, the transition is first order. In the absence of evidence to the contrary, it is assumed to be second order. In practice, it can be very difficult to make this distinction as is well illustrated by the investigations of the paramagnetic to ferromagnetic transition in manganite systems such as $La_{1-x}Ca_xMnO_3$, a subject reviewed by Biernacki [2]. In this investigation, we consider only doping levels near $x = 0.3$ where the only phases present are paramagnetic and ferromagnetic.

* Corresponding author. Email: james.loudon@physics.org

Nearly all paramagnetic to ferromagnetic phase transitions are second order. Only a few first order transitions have been observed, notably in MnAs where the Curie temperature is found to differ by 10 K on warming compared with cooling when the magnetisation is measured as a function of temperature [3]. In conventional magnetisation experiments, any such thermal hysteresis in $La_{0.7}Ca_{0.3}MnO_3$ is much smaller (see figure 1) and the magnetisation in $La_{2/3}Ca_{1/3}MnO_3$ appears to diminish gradually and continuously as is conventional for a second order transition [4]. This is not conclusive evidence that the phase transition is second order, however, because the magnetisation is averaged over the specimen and a gradual reduction in magnetisation on warming could be caused either by a reduction in the local magnetisation uniformly throughout the specimen (as in a second order transition) or the growth of paramagnetic patches within the ferromagnetic phase (a first order transition). Thus researchers turned to other methods to make the distinction.

In the ideal second order phase transition envisioned by Ehrenfest [5], there should be a finite step in the heat capacity at the transition temperature. However, following the theoretical work of Onsager [6] on a two dimensional Ising model of a ferromagnet, it is now thought that a lambda anomaly should be observed at a ferromagnetic transition where the heat capacity tends to infinity at the transition temperature but the temperature continues to rise as heat is applied so there is no latent heat. In practice, the heat capacity peak does not rise to infinity at the transition point during a ferromagnetic phase transition and this is usually accounted for by the presence of defects within the sample and the finite temperature resolution of the equipment [7].

This qualification makes it harder to distinguish first and second order transitions from heat capacity measurements as the latent heat present in a first order transition also causes an infinite peak in the heat capacity. However, the lambda anomalies observed in second order transitions are asymmetric and it is usual to argue that the more symmetric the peak, the more likely the transition is to be first order.

In 1997, Zhao *et al.* [8] investigated the heat capacity of $La_{0.67}Ca_{0.33}MnO_3$ and interpreted their results using Ehrenfest's equations for a second order transition. They concluded that the transition was indeed second order. However, Gordon *et al.* [9] later found that the heat capacity peak at the Curie point of $La_{0.65}Ca_{0.35}MnO_3$ was unusually symmetric and could not be fitted by curves based on fluctuation theories used to account for the behaviour of conventional ferromagnets. They therefore argued that the transition was first order. The same observation was made by Mira *et al.* [10] who found that the peak was very symmetrical for $La_{2/3}Ca_{1/3}MnO_3$ but, interestingly, was asymmetric and typical of a conventional second order Curie transition in $La_{2/3}Sr_{1/3}MnO_3$.

Further evidence for a first order ferromagnetic transition in $La_{0.67}Ca_{0.33}MnO_3$ came from small angle neutron scattering experiments conducted by Lynn *et al.* [4] who observed that the spin stiffness did not tend to zero at the Curie temperature, unlike a conventional ferromagnet. They also observed a 5 K thermal hysteresis in the magnetisation measured by neutron diffraction. They interpreted this as evidence of a coexistence of paramagnetic and ferromagnetic phases near the Curie point and hence a first order transition. It should be noted that such hysteresis has not been widely reported by other authors and our own magnetisation measurements (see figure 1)

made with a vibrating sample magnetometer indicate that any thermal hysteresis is less than 2 K. This discrepancy is probably due to the long relaxation times required for the magnetisation to reach equilibrium observed by Adams *et al.* [11] as well as the fact that the our measurements were made in a field of 1T whereas the neutron diffraction measurements were made in zero field. Adams *et al.* show that if the sample is warmed and cooled sufficiently slowly, there is no hysteresis. The authors described the phase transition as weakly first order.

Whilst it is now generally accepted that the ferromagnetic phase transition is first order in $La_{1-x}Ca_xMnO_3$ near $x = 0.3$ (although it is thought to be second order for $x = 0.2$ [11] and $x = 0.4$ [12]), the ferromagnetic transition in $La_{1-x}Sr_xMnO_3$ was thought to be second order at all compositions $0.2 < x < 0.5$ [12]. It therefore came as a surprise that a microscopic study by Yoo *et al.* [13] of $La_{0.81}Sr_{0.19}MnO_3$ using electron holography identified ferromagnetic clusters in a paramagnetic background near its Curie temperature despite the fact this compound that has the same structure and phases as $La_{0.80}Sr_{0.20}MnO_3$ [14] where a second order phase transition was identified on thermodynamic grounds [15].

This illustrates both the difficulty of identifying the nature of the phase transition and the value of microscopic measurements. Electron holography has the great advantage of giving a quantitative, local measurement of the order parameter (magnetisation) during the ferromagnetic transition. In order to clarify the nature of the ferromagnetic phase transitions that can occur in the manganites, we have conducted a study of the paramagnetic to ferromagnetic transition in $La_{0.7}Ca_{0.3}MnO_3$ using electron holography. We find that rather than exhibiting characteristics of a pure first or second order transition, it exhibits features of both. As the sample is warmed from 90K towards its Curie temperature (257 K), the local magnetisation diminishes in a uniform, continuous manner until 242 K where the behaviour changes dramatically. The magnetic domains shrink away from the edges of the specimen leaving paramagnetic regions behind. Fresnel imaging shows that the domains retreat to grain boundaries in the material and then vanish in a discontinuous manner. This process is reversed on cooling. In contrast, the magnetisation in nickel fades uniformly and continuously with increasing temperature, vanishing completely at the Curie point.

2. Experimental Details

2.1. *Sample synthesis and preparation*

The sample of $La_{0.7}Ca_{0.3}MnO_3$ used in this investigation was synthesised by A.J. Williams at the Chemical Laboratory, Cambridge University. It was prepared by repeated grinding, pressing and sintering of La_2O_3, $CaCO_3$ and MnO_2 in stoichiometric proportions. The La_2O_3 was heated overnight prior to use in order to dehydrate it. The sample was prepared by heating initially at 950°C for 12 hours to decarboxylate the $CaCO_3$, and then at 1350°C for 12 hours. The sample was then reground, repelleted and heated at 1350°C for 4 days; and then reground, repelleted and reheated at 1300°C for 2 days. The final sample was a polycrystal with a grain size of 5μm. X-ray powder diffraction and energy dispersive x-ray analysis using a scanning electron microscope confirmed the presence of a single phase. Large area (10×10 μm) energy dispersive x-ray analysis showed that the La/Ca ratio was constant to within the error of the measurements ($\delta x = \pm 2$ %). The sample was

prepared for transmission electron microscopy by conventional mechanical polishing and argon ion thinning at liquid nitrogen temperatures using a Gatan Duo Mill ion thinner.

The single crystal nickel sample was made by K. Roberts at the Department of Materials Science and Metallurgy, Cambridge University using the Bridgman floating zone technique [16]. It was prepared for transmission electron microscopy by electropolishing at room temperature in a 5% solution of perchloric acid in butoxyethanol.

2.2. *Magnetometry*

The magnetisation of $La_{0.7}Ca_{0.3}MnO_3$ was measured with a Princeton Measurements Corporation "Micromag" vibrating sample magnetometer equipped with a liquid helium cooled cryostat. The magnetisation was measured as a function of temperature between 50 and 300 K in a field of 1 T, chosen so that the sample was magnetically saturated at all temperatures. Warming and cooling was performed at a rate of 4 K/minute to minimise the effects of thermal inertia. The sample volume was measured by weighing the sample with a four figure balance and converting this to a volume via the known density. The uncertainty in the sample mass was 0.5 % and this was the principal uncertainty in the magnetisation measurement.

2.3. *Transmission electron microscopy*

Transmission electron microscopy was undertaken using a 300 kV Philips CM300 microscope equipped with a field emission gun to provide a coherent source of electrons, an electron biprism used for holography and a 'Lorentz' lens (a strong objective mini lens) which allowed the magnetic structure of a specimen to be observed in near-zero (less than 0.02 T) magnetic field. A Gatan model 636 double tilt liquid nitrogen cooled specimen stage was used to cool the samples to 90 K. Heating experiments were performed with a Philips PW6592 single tilt heating holder.

Two methods were used to image the magnetic structure of the material: Fresnel imaging and electron holography. In the Fresnel method [17] the sample is imaged out of focus with a coherent beam of electrons. Lorentz forces in the sample cause magnetic domain walls to appear as bright interference fringes where the electrons converge and dark regions where the electrons diverge.

To acquire electron holograms [18], an electron biprism (a positively charged wire) is inserted into the column of the microscope and used to interfere a reference wave passing through vacuum with one passing through the sample. A digital reconstruction allows both the amplitude and phase of the exit wavefunction to be determined directly.

Taking coordinates x and y normal to the beam direction z, the phase change on passing through the specimen is given by [19]

$$\phi(x,y) = C_E \int V_0(x,y,z)\,\mathrm{d}\,z - \frac{2\pi e}{h}\iint \mathbf{B}_\perp(x,y,z)\cdot\mathbf{dS} \qquad (1)$$

where $C_E = \frac{2\pi e}{\lambda}\left(\frac{eV + mc^2}{eV(eV + 2mc^2)}\right) = 6.523 \times 10^6$ m^{-1}V^{-1} for $V = 300$ kV, e is the electron charge, m is the electron rest mass, V is the acceleration voltage = 300 kV, c is the speed of light, λ is the wavelength of an electron = 0.0197 Å at 300 kV, $V_0(x,y,z)$ is the mean inner potential, $\mathbf{B}_\perp(x, y, z)$ is the component of magnetic flux density normal to the electron beam and **dS** is an element of vector area normal to the beam direction. This formula holds true provided that the specimen is not diffracting strongly. This is ensured by tilting away from any major zone axes.

By comparing holograms taken above the Curie temperature, T_C with those taken below, we can rearrange equation (1) to give a measure of the absolute value of the magnetisation in a way that does not depend on the unknown thickness of the sample:

$$\mu_0 \mathbf{M}_\perp(x, y) = \mathbf{B}_\perp(x, y) = -\frac{h}{2\pi e} C_E V_0 \frac{1}{\phi_{T>T_C}(x, y)} \begin{pmatrix} \partial/\partial y \\ -\partial/\partial x \end{pmatrix} \left\{ \phi_{T<T_C}(x, y) - \phi_{T>T_C}(x, y) \right\} \quad (2)$$

This formula assumes that: (1) V_0 is constant throughout the sample and has the value of 23.80 V for $La_{0.7}Ca_{0.3}MnO_3$ and 28.70 V for nickel calculated from electron scattering factors [20], (2) $\mathbf{B}_\perp(x, y)$ is constant throughout the thickness of the sample and (3) demagnetising effects are negligible so that the magnetisation is directly proportional to the flux density (we investigate this assumption in section 3.2). The specimen preparation for transmission electron microscopy yielded thin (thickness ~150 nm), continuous films and thus we expect the shape anisotropy ($\frac{1}{2}\mu_0 M^2 = 2.5 \times 10^5$ J m^{-3}) to force the magnetisation to lie in the plane of the film (perpendicular to the electron beam) since the uniaxial magnetocrystalline anisotropy energy is considerably smaller, $K \sim 10^3$–10^4 J m^{-3} [21, 22].

3. Results

3.1. *$La_{0.7}Ca_{0.3}MnO_3$*

The magnetisation of $La_{0.7}Ca_{0.3}MnO_3$ was measured as a function of temperature with a vibrating sample magnetometer under an applied field of 1T as shown in figure 1. It can be seen that the magnetisation rises on cooling and has a value 3.71 ± 0.02 μ_B/Mn (the theoretical spin-aligned value is 3.70 μ_B/Mn) at 50 K. The Curie temperature (judged by the inflexion point on the curve) was 257 K. The sample temperature was changed at 4 K/min in order to reduce thermal inertia as far as was practicable and a comparison of warming and cooling curves gave an upper bound of 2 K on any thermal hysteresis. At 90 K, the lowest temperature accessible with the liquid nitrogen cooled specimen stage for the electron microscope, the magnetisation was 3.65 ± 0.02 μ_B/Mn.

[Insert figure 1 about here]

We then measured the local magnetisation using electron holography as described in the section 2.3. For each hologram, we measured the magnetisation in around 10 0.1 μm square regions. From these we found the average magnetisation and random error associated with this measurement.

The mean inner potential V_0 was derived from electron scattering factors, assuming that all the atoms are neutral and no bonding takes place. This assumption is likely to overestimate V_0 and thus the magnetisation, possibly by as much as 10%. This systematic error is present for all our measurements and so will only affect the absolute values of the magnetisation not the relative values when comparing the magnetisation in holograms from the same specimen at different temperatures.

Figure 2(a) shows the arrangement of magnetic domains at 90 K. It can be seen that they are separated by 180° domain walls and have triangular 90° closure domains at the specimen edge. This is a typical magnetic structure of a ferromagnet. The magnetisation measured by electron holography at this temperature was 3.61 ± 0.08 μ_B/Mn, in good agreement with the bulk magnetisation of 3.65 ± 0.02 μ_B/Mn measured by vibrating sample magnetometry.

As the specimen was warmed, the domain structure changed very little. Figure 2(b) taken at 242 K shows a cooperative movement of the domains with respect to (a) but the shapes and sizes of the domains are very similar. Such rearrangements in the magnetic structure frequently occur as a magnetic specimen is warmed (see section 3.2). It will also be noted that there is a small black region near the edge of the specimen indicating that the specimen has become paramagnetic in this region. The most striking difference is that the apparent local magnetisation has reduced to 1.67 ± 0.04 μ_B/Mn in the ferromagnetic regions. We refer to this measurement as an 'apparent' magnetisation because it was made in projection and assumes that the magnetisation is uniform throughout the thickness of the specimen. However, it is likely that there were paramagnetic regions above and below the ferromagnetic phase which reduce the measured magnetisation (see section 3.1.1.3).

Only 1 K higher at 243 K, the ferromagnetic regions began a more rapid withdrawal from the edge of the specimen and figures (b) to (d) chart the progress of this withdrawal. In figure 2(c), the apparent local magnetisation in the ferromagnetic regions has fallen to 1.46 ± 0.04 μ_B/Mn and in (d) at 244 K, the ferromagnetic region has an apparent local magnetisation of 1.23 ± 0.03 μ_B/Mn. Above 244 K, the ferromagnetic phase is no longer visible in this region of the sample. The local magnetisation of single crystal nickel is shown for comparison in panels (e)–(h) and discussed in section 3.2.

[Insert figure 2 about here]

In order to gain a better insight into the processes that took place near the Curie point, Fresnel images were recorded as videos. The Fresnel technique is less quantitative than off axis holography, but images can be acquired much faster and larger areas can be imaged since the size of the image is not limited by the size of the interference region from the biprism. They can also be recorded far from the specimen edge unlike holography where the vacuum is used as a reference.

The nucleation and growth of magnetic domains is shown in Figures 3(a)–(h). As the specimen was cooled through its Curie temperature, magnetic domains formed first on a grain boundary and then spread into the bulk of the specimen. Further Fresnel measurements showed that as the specimen was warmed, this process was reversed: magnetic domains withdrew from the specimen edge towards grain boundaries where

they finally disappeared. The growth of the domains is not a continuous process but proceeds by a series of discontinuous expansions which take place faster than the frame rate of the video (< 1/15 s). We have also found that the slower the temperature is changed, the slower the transition takes place.

[Insert figure 3 about here]

The Fresnel imaging also provided a reliability check for the temperature measurement. We found that to within 2 K, the thermocouple on the liquid nitrogen cooled specimen stage recorded the same temperature when the phase transition took place both on warming and cooling. Changing the convergence angle of the electron beam did not have any significant effect on the temperature at which the transition took place so heating by the electron beam was not significant for the conditions used here. We are thus confident that the temperatures recorded are an accurate measurement of the specimen temperature to within 2 K.

Thus, the transition appears to progress first by a gradual, uniform fading of the magnetisation characteristic of a second order transition followed by a first order withdrawal of the ferromagnetic regions from the specimen edge so that paramagnetic and ferromagnetic phases coexist at the same temperature.

3.1.1 Other possible interpretations

In the previous section we found that the paramagnetic to ferromagnetic transition in $La_{0.7}Ca_{0.3}MnO_3$ appeared to be neither a pure first or second order transition but seemed to be a mixture of both. We now consider whether the transition could be a pure first or second order transition and whether the nature of our measurements could have led us to an incorrect conclusion.

3.1.1.1 Ion beam damage leading to variable Curie temperatures

The first possibility is that the transition is second order but the ion beam thinning used in the sample preparation caused the Curie temperature near the specimen surface to be reduced as illustrated in figure 4. In order to observe a withdrawal of the magnetisation from the edge of the specimen, the Curie temperature would have to vary continuously with depth.

[Insert figure 4 about here]

This scenario appears to explain the observed behaviour: when viewed along the beam direction, the magnetisation would first occur in the thicker regions of the sample and then spread towards the edges as the temperature is reduced. It is not consistent with the Fresnel images in figure 3, however, which show the ferromagnetic phase first forming near where a grain boundary reaches the specimen edge and then spreading along the grain boundary into a *thicker* part of the specimen.

Furthermore, in this model, it would also be necessary to assume that the grain boundaries had the highest Curie temperature since this is where the ferromagnetic phase first forms. Thus we would need to assert on the one hand that atomic disorder caused by ion thinning caused a reduction of the Curie temperature but the atomic disorder that arises from the presence of a grain boundary *increases* the Curie

temperature above that of the bulk. We therefore consider it unlikely that ion thinning is responsible for the effects observed here

3.1.1.2 Differing temperatures throughout the sample

Another point that requires consideration is how the temperature varies throughout the sample. If grain boundaries conducted heat more efficiently than the bulk of the sample, that would explain why the magnetisation appears first on grain boundaries as the specimen is cooled. However, if this were the case, on heating the grain boundaries would be warmer than the surrounding sample and the magnetisation would vanish first at the boundaries. This is not observed: on warming, the grain boundaries become paramagnetic last. Therefore the nucleation and growth we observe is not an artefact of differing temperatures in the sample.

3.1.1.3 Nucleation of paramagnetic phase at all surfaces

So far, we have been assuming that the paramagnetic phase forms at the sample edge. We now consider the possibility that the paramagnetic phase forms at all sample surfaces, i.e. above and below the ferromagnetic region as illustrated by the schematic cross section in figure 5. We can estimate the thickness, t, of the paramagnetic layer from the width, w, of the paramagnetic region surrounding the ferromagnetic region observed by electron holography via

$$t = w\sin(\theta/2) \tag{3}$$

where θ is the wedge angle found from holograms taken above the Curie temperature where the phase shift can be directly related to the sample thickness. Knowing the thickness of the paramagnetic region, t, and the total sample thickness, the true magnetisation, M can be estimated from the apparent magnetization, M^* as summarised in table 1. This analysis shows that the corrected magnetisation in the ferromagnetic regions is in reasonable agreement with the bulk magnetisation of 2.50 ± 0.01 μ_B/Mn measured by vibrating sample magnetometry. It is thus likely that the paramagnetic phase forms at all sample surfaces before spreading into the bulk of the material. (In making this comparison, we assume that the bulk magnetisation is unaffected by the 20–40 nm of paramagnetic material at the surface.)

[Insert figure 5 about here]

[Insert table 1 about here]

Thus our microscopic investigation has shown that only a thin layer (< 20 nm) of the paramagnetic phase is present at temperatures below 242 K and thus the bulk magnetisation measured by vibrating sample magnetometry gives the magnetisation of the ferromagnetic phase in this temperature range. Above 244 K, the bulk magnetisation is averaged over both the ferromagnetic and paramagnetic phases. We have indicated this in figure 1 with a dotted line: at temperatures below the dotted line the volume fraction of the paramagnetic phase is so small that the measured magnetisation is that of the ferromagnetic phase. The magnetisation curve shows that as the specimen is warmed, the magnetisation reduces continuously before phase

separation occurs. This continuous reduction in magnetisation anticipates the first order transition: a so-called premonitory effect [23]. We therefore describe the transition is a combination of first and second order processes.

3.1.2 The ferromagnetic transition in $La_{0.7}Ca_{0.3}MnO_3$: conclusions

From our study thus far, we conclude that the ferromagnetic to paramagnetic transition which takes place in $La_{0.7}Ca_{0.3}MnO_3$ is primarily a first order transition. The transition itself is preceded by a continuous reduction in magnetisation. This anticipation of the first order transition is reminiscent of the premonitory effects observed in other first order phase transitions [23] such as the appearance of a 'tweed' microstructure which precedes a martensitic phase transformation [24].

As the specimen is warmed towards its Curie temperature, the paramagnetic phase forms on the specimen surface and grows into the bulk of the specimen and the ferromagnetic phase retreats towards grain boundaries where it disappears in a series of discontinuous changes. On cooling, the ferromagnetic phase forms on the same grain boundaries and spreads into the bulk, driving the paramagnetic phase to the specimen surfaces.

Thus, both the ferromagnetic and paramagnetic phases form on surfaces (either grain boundaries or the specimen surface) before spreading into the bulk of the specimen. This heterogeneous nucleation is not unexpected as the growth of the new phase can take place with a substantially lower energy cost than an equivalent homogeneous route from the interior of a grain. We note that in the absence of suitable surfaces, point nucleation of the ferromagnetic phase can occur as has been observed in single crystal $La_{0.46}Sr_{0.54}MnO_3$ by Murakami *et al.* using electron holography [25].

It is rather surprising that the ferromagnetic phase forms on grain boundaries but the paramagnetic phase forms on the specimen surfaces: one might have thought that the same nucleation sites would serve for either phase. At present, we are unclear as to why this is the case. In the future we plan to use electron holography to clarify this issue by investigating the magnetisation distribution of the ferromagnetic phase as it forms on grain boundaries. Although all our results indicate that the paramagnetic phase forms at the free surfaces of the specimen, it is possible that other nucleation sites become more favourable for thicker specimens as the surface area to volume ratio becomes smaller.

3.2. *Single crystal nickel*

In order to further check the validity of our interpretation, we performed a similar experiment with single crystal nickel which should display a conventional second order ferromagnetic to paramagnetic phase transition and which should be readily distinguishable from the phase transition observed in $La_{0.7}Ca_{0.3}MnO_3$. The specimen preparation (see section 2.1) yielded a sample with a similar geometry to that of the manganite. The <100> direction was normal to the plane of the film and since nickel has four fold magnetocrystalline anisotropy, we also expect the magnetisation to lie in the plane of the film. Nickel has a Curie temperature of 631 K and a saturation magnetisation of 0.60 T at 300 K [26]; the magnetisation tends towards a limit of 0.61 T as the temperature approaches 0 K [27].

At room temperature (296 K), the magnetisation measured by electron holography was 0.60 ± 0.02 T in good agreement with the bulk value. It can be seen from figure 2(e)–(h) that like the manganite sample, the magnetisation fades gradually and uniformly and rearrangements of the magnetic structure take place during this process. However, unlike the manganite sample, there is no withdrawal of the domains from the specimen edge: the magnetisation simply fades away with increasing temperature as expected in a second order phase transition.

It is interesting to note that the magnetisation does not appear to fade at the same rate in every domain. The domain marked B in figure 2(f) was 20% more magnetic than the surrounding domains at 447 K. This is unexpected because in a second order phase transition, the entire sample should have the same magnetisation throughout. Figure 6 shows a graph of the magnetisation measured in A and B as a function of temperature.

[Insert figure 6 about here]

We now consider whether the apparent difference in magnetisation between domains A and B at the same temperature is real or an artefact of our measurement technique. The most obvious possibility is that the sample is tilted so that we measure the full magnetisation in domain B but only a component of the magnetisation in domain A as illustrated in figure 7.

[Insert figure 7 about here]

If the sample were tilted in this manner, we could find the tilting angle from the ratio of the magnetisation in domains A and B. If this explanation is correct, the ratio should remain constant with temperature. In fact, as shown in figure 8, the ratio of magnetisation does change with temperature and if the sample were indeed tilted, θ would need to change from 35° to 20° to account for this effect. It is very unlikely that sample was tilted by this large angle and the fact that the ratio changes systematically with temperature indicates that this is not the cause of the discrepancy.

[Insert figure 8 about here]

Thus far, we have assumed that the magnetisation **M** is equal to the flux density **B**. This assumes that the magnetic field strength **H** within the specimen is negligible which we expect because the domain structure should minimise the number of magnetic poles at the specimen edge which give rise to **H**. However, a small stray field can be observed in the vacuum implying that there are some magnetic poles at the specimen edge (see figure 9).

In order to investigate the distribution of fields in the sample, we have simulated a domain structure that matches the observed domain structure and which has a constant magnetisation in each domain. The simulations were based on the equations given by Beleggia and Zhu [28] which allow a direct calculation of the phase shift that an electron beam suffers as it traverses a sample. For a sample with a constant magnetisation and the electron beam in the z direction, the magnetic contribution to

the phase shift $\phi(x,y)$ can be evaluated from the inverse Fourier transform of the following function:

$$\tilde{\phi}(k_x,k_y) = i\frac{e}{\hbar}\mu_0 M \frac{\tilde{T}(k_x,k_y)}{k^2}(\hat{\mathbf{m}}\times\mathbf{k})_z \quad (4)$$

where M is the magnitude of the magnetisation and $\hat{\mathbf{m}}$ is a unit vector in the direction of the magnetisation. The subscript z indicates that $\hat{\mathbf{m}}\times\mathbf{k}$ is to be evaluated in the z direction only. The function $T(x,y)$ is the thickness of the specimen normal to he electron beam and $\tilde{T}(k_x,k_y)$ its Fourier transform. In this notation, the forward transform is defined as

$$\tilde{T}(k_x,k_y) = \int T(x,y)e^{-i(k_x x+k_y y)}dxdy \quad (5)$$

A sample with several domains can be simulated by performing separate calculations for each magnetisation direction and then summing the resultant phases, ϕ, from each direction. Figure 9 shows a comparison of simulated data and experimental data for the magnetic phase shift associated with the specimen. We find that the apparent magnetisation measured by the method explained in section 2.3 is indeed different in domains A and B although we input the same magnetisation into each domain in the simulation. The ratio of the simulated apparent magnetisations in A and B is 0.85, which agrees rather well with experimental value of 0.81 ± 0.03 given the approximations used. It would appear therefore that the difference in magnetisations can be explained as a systematic error in our measurement of the magnetisation due to neglecting the **H** field. It should be noted that simulations for the 180° domains observed in the manganite sample indicate that the systematic error in our measurement of the magnetisation is much smaller.

[Insert figure 9 about here]

However, we would also expect the ratio of the apparent magnetisations to remain constant with temperature if demagnetising effects were the cause of the discrepancy since the shape of the domains remains very similar as the specimen is heated and the magnetisation is meant to reduce homogeneously in a second order transition. However, as in indicated in figure 8(a), the ratio is not constant but gradually approaches unity as the temperature is increased even though the domain configuration hardly changes. We are unable to account for this effect at present but conclude that we have no evidence that the ferromagnetic transition in nickel is anything other than a purely continuous phase transition.

4. Conclusions

Many investigations have been made to determine whether the paramagnetic to ferromagnetic transition observed in the manganites is first or second order and, as explained in the introduction, the results are controversial. Our holographic measurements of the local magnetisation have shown that the transition in $La_{0.7}Ca_{0.3}MnO_3$ is not purely first or second order but shows features of both. As the specimen is warmed towards its Curie point, the magnetisation falls homogeneously

until it reaches about three quarters of its spin-aligned value. At this point, the magnetic domains withdraw leaving paramagnetic material behind. We have observed the domains withdrawing in a series of rapid, discontinuous movements from the specimen edge to a grain boundary and then disappearing, one by one. This process is reversed on cooling through the Curie point. We did not observe nucleation of the ferromagnetic phase at point defects but expect that in the absence of planar defects, point defects would act as nucleation sites. Indeed, Murakami *et al.* [25] have observed nucleation of magnetic domains from a point in single crystal $La_{0.46}Sr_{0.54}MnO_3$. The speed of the withdrawal of the domains appears to be governed entirely by the warming rate and we believe that if held at a certain temperature, the domain configuration will remain static. In contrast, the ferromagnetic transition in nickel appears to be a purely continuous process.

Bean and Rodbell [29] investigated the theoretical possibility of a first order ferromagnetic to paramagnetic phase transition and concluded that if the crystal lattice is compressible and the magnetic exchange energy depends sufficiently strongly on the bond lengths between the atoms, a first order transition may occur. Radaelli *et al.* [30] have shown that the Mn-O bond length changes suddenly at the Curie point of $La_{0.75}Ca_{0.25}MnO_3$ indicating that the structural degrees of freedom are strongly coupled to the magnetic degrees of freedom. We suggest that this coupling results in the first order phase transition observed in $La_{0.7}Ca_{0.3}MnO_3$. In contrast, no similar dependence exists in nickel which is why its phase transition appears to be continuous.

5. References

1. L.D. Landau and E.M. Lifshitz, *Statistical Physics*, (Permagon Press, London, 1958).
2. S.W. Biernacki, Phys. Rev. B **68** 174417 (2003).
3. L.F. Bates Proc. Roy. Soc. A **117** 778 680 (1928).
4. J.W. Lynn, R.W. Erwin, J.A. Borchers, Q. Huang, A. Santoro, J-L. Peng, Z.Y. Li Phys. Rev. Lett. **76** 21 4046 (1996).
5. P. Ehrenfest Lieden Comm. Suppl. **75b** (1933).
6. L. Onsager Phys. Rev. **65** 3, 4 117 (1944).
7. D.L. Connelly, J.S. Loomis, D.E. Mapother, Phys. Rev. B **3** 3 924 (1971).
8. G.M. Zhao, M.B. Hunt, H. Keller, Phys. Rev. Lett. **78** 955 (1997).
9. J.E. Gordon, C. Marcenat, J.P. Franck, I. Isaac, G. Zhang, R. Lortz, C. Meinqast, F. Bouquet, R.A. Fisher, N.E. Phillips, Phys. Rev. B **65** 024441 (2001).
10. J. Mira, J. Rivas, L.E. Hueso, F. Rivadulla, M. A. López Quintela, M. A. Señarís Rodríguez, C.A. Ramos, Phys. Rev. B **65** 024418 (2002).
11. C.P. Adams, J.W. Lynn, V.N. Smolyaninova, A. Biswas, R.L. Greene, W. Ratcliff, S-W. Cheong, Y. M. Mukovskii, D. A. Shulyatev, Phys. Rev. B **70** 134414 (2004).
12. D. Kim, B. Revaz, B.L. Zink, F. Hellman, J.J. Rhyne, J.F. Mitchell, Phys. Rev. Lett. **89** 22 227202 (2002).
13. J.H. Yoo, Y. Murakami, D. Shindo, T. Atou, M. Kikuchi, Phys. Rev. Lett. **93** 4 047204 (2004).

14. M. Paraskevopoulos, F. Mayr, C. Hartinger, A. Pimenov, J. Hemberger, P. Lunkenheimer, A. Loidl, A.A. Mukhin, V.Y. Ivanov, A.M. Balbashov, J. Mag. Mag. Mat. **211** 118 (2000).
15. D. Kim, B.L. Zink, F. Hellman, J.M.D. Coey, Phys Rev B **65** 214424 (2002).
16. J.C. Brice, *Crystal Growth Processes*, (Blackie, Glasgow, 1986).
17. P. Hirsh, A. Howie, R. Nicholson, D. W. Pashley, M. J. Whelan *Electron Microscopy of Thin Crystals,* revised edtn. (Krieger Publishing Company, Florida, USA, 1977).
18. P.A. Midgley *Micron* **32** 167 (2001).
19. R.E. Dunin-Borkowski, M.R. McCartney, D.J. Smith, S.S.P. Parkin *Ultramicroscopy* **74** 61 (1998).
20. D. Rez, P. Rez, I. Grant, Acta. Cryst. A **50** 481 (1994).
21. Y. Suzuki, H.Y. Hwang, S-W. Cheong, T. Siegrist, R.B. van Dover, A. Asamitsu, Y. Tokura, J. Appl. Phys. **83** 11 7064 (1998).
22. V. Markovich, E. Rozenberg, A. I. Shames, G. Gorodetsky, I. Fita, K. Suzuki, R. Puzniak, D.A. Shulyatev, Ya. M. Mukovskii, Phys. Rev. B **65** 144402 (2002).
23. A. Putnis, *Introduction to Mineral Sciences* (C.U.P., Cambridge, 1995).
24. S. Kartha, J.A. Krumhansi, J.P. Sethna, L.K. Wickham, Phys. Rev. B **52** 2 803 (1995).
25. Y. Murakami, J.H. Yoo, D. Shindo, T. Atou, M. Kikuchi, Nature **423** 965 (2003).
26. D. Jiles, *Introduction to Magnetism and Magnetic Materials* (Chapman and Hall, London, 1991).
27. R.C. Weast (Editor) *Handbook of Chemistry and Physics* 57th edtn., The Chemical Rubber Company, 1973.
28. M. Beleggia and Y. Zhu, Phil. Mag. **83** 8 1045 (2003).
29. C.P. Bean and D.S. Rodbell Phys. Rev. **126** 1 102 (1962).
30. P. G. Radaelli, G. Iannone, M. Marezio, H.Y. Hwang, S.-W. Cheong, J.D. Jorgensen, D.N. Argyriou, Phys. Rev. B **56** 13 8265 (1997).

Table Captions

Table 1. The average apparent magnetisation M^* in $La_{0.7}Ca_{0.3}MnO_3$ can be corrected for the thickness of the paramagnetic layer, t, to give an estimate of the true magnetisation, M, as described in the text.

Figure Captions

Figure 1. Magnetisation versus temperature for $La_{0.7}Ca_{0.3}MnO_3$ in a field of 1 T as measured by vibrating sample magnetometry. Warming and cooling curves are included in the plot although these very nearly coincide giving an upper bound of 2 K on any thermal hysteresis. Transmission electron microscopy revealed that the magnetisation reduced homogeneously with increasing temperature in the range marked 'homogeneous'. Above 242 K (marked by the dashed line), ferromagnetic and paramagnetic phases coexisted (see text).

Figure 2(a)-(d): The disappearance of ferromagnetism in $La_{0.7}Ca_{0.3}MnO_3$ measured by electron holography as the sample was warmed towards its Curie point of 257 K. Ferromagnetic regions are coloured with the direction of magnetisation indicated by the colour wheel in the inset to (b) as well as by arrows superimposed. The strength of the magnetisation is indicated by the intensity of the colour. Note that electron holograms only give information near the specimen edge and the specimen continues into the lower right hand corner of each panel marked `specimen interior'. The temperature (T) and the average apparent magnetization (M^*) in each image is (a) $T = 90$ K, $M^* = 3.61 \pm 0.08$ μ_B/Mn, (b) $T = 242$ K, $M^* = 1.67 \pm 0.04$ μ_B/Mn, (c) $T = 243$ K, $M^* = 1.46 \pm 0.04$ μ_B/Mn, (d) $T = 244$ K, $M^* = 1.23 \pm 0.03$ μ_B/Mn . (e)-(h): The development of magnetisation in single crystal nickel. (e) $T = 294$ K, $M = 0.59 \pm 0.02$ T, (f) $T = 447$ K, $M = 0.56 \pm 0.03$ T, (g) $T = 632$ K, $M = 0.17 \pm 0.01$ T, (h) T = 634 K, no detectable ferromagnetism.

Figure 3. Fresnel images taken from a video as the specimen was cooled through its Curie temperature at a rate of 2 K/minute starting at 243 K (a) 0 s, (b) 7 s, (c) 13 s, (d) 20 s, (e) 27 s, (f) 33 s, (g) 40 s (h) 47 s. The images have been enhanced by averaging over 10 frames (0.7 seconds) and high pass filtering. A grain boundary runs between the arrows in (a). Magnetic domain walls appear as bright and dark lines (indicated by arrows in (h)) which spread from the grain boundary towards the left of the figure.

Figure 4. Schematic cross sectional view of the sample illustrating the scenario where ion beam damage leads to a reduction in the Curie temperature (T_C) near the surface of the specimen.

Figure 5. Schematic cross section of the $La_{0.7}Ca_{0.3}MnO_3$ sample showing the relationship between the width of the paramagnetic region measured in projection by electron holography, w, and the thickness of the paramagnetic layer, t, assuming that the paramagnetic layer grows from all surfaces. FM and PM stand for ferromagnetic and paramagnetic respectively.

Figure 6. Graph showing the apparent magnetisation in domains A and B measured on warming and the average for the two domains (error bars are comparable with the size of the points). The data for the bulk magnetisation in zero field was taken from ref. 30.

Figure 7. Schematic cross section of the sample showing that sample tilt could give an apparent magnetisation in domain A which was less than that in B.

Figure 8. (a) Ratio of magnetisation in domain A to that in B as a function of temperature. (b) The angle θ through which the specimen would need to be tilted to produce this ratio. The dashed line is a guide to the eye.

Figure 9. (a) The cosine of four times the magnetic contribution to the phase shift observed experimentally. (b) Simulation of the phase shift associated with the magnetic domains assuming each has the same magnetisation. The thickness profile used in the simulation was based on the experimental thickness profile averaged vertically. The slope of the thickness profile actually has a vertical component which

is why the lines in domain B are at a different angle in (a) and (b). Note that Néel domain walls of width 20 nm were used in the simulations as this was computationally more convenient than the Bloch walls which are more likely to occur. (c) The modulus of the experimental magnetisation calculated using the method described in section 2.3. (d) The modulus of the magnetisation from the simulation calculated using the method described in section 2.3 shows that the apparent magnetisation in domain B is higher than that in A although the simulation has the same magnetisation in each domain.

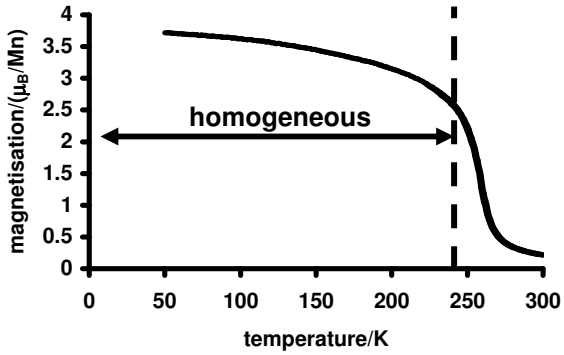

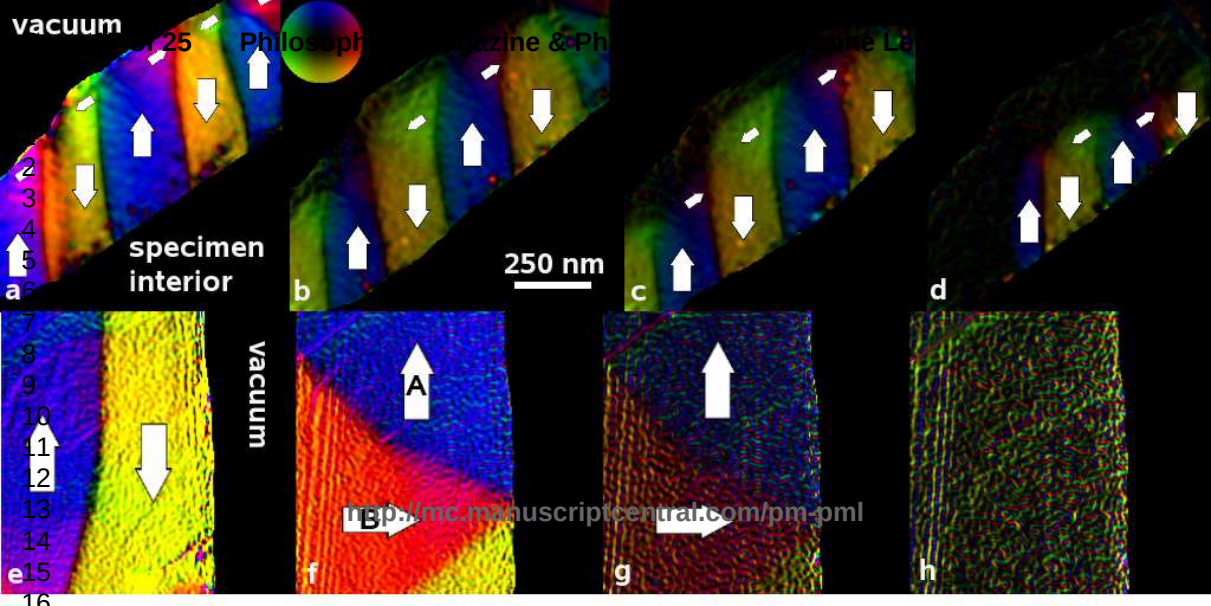

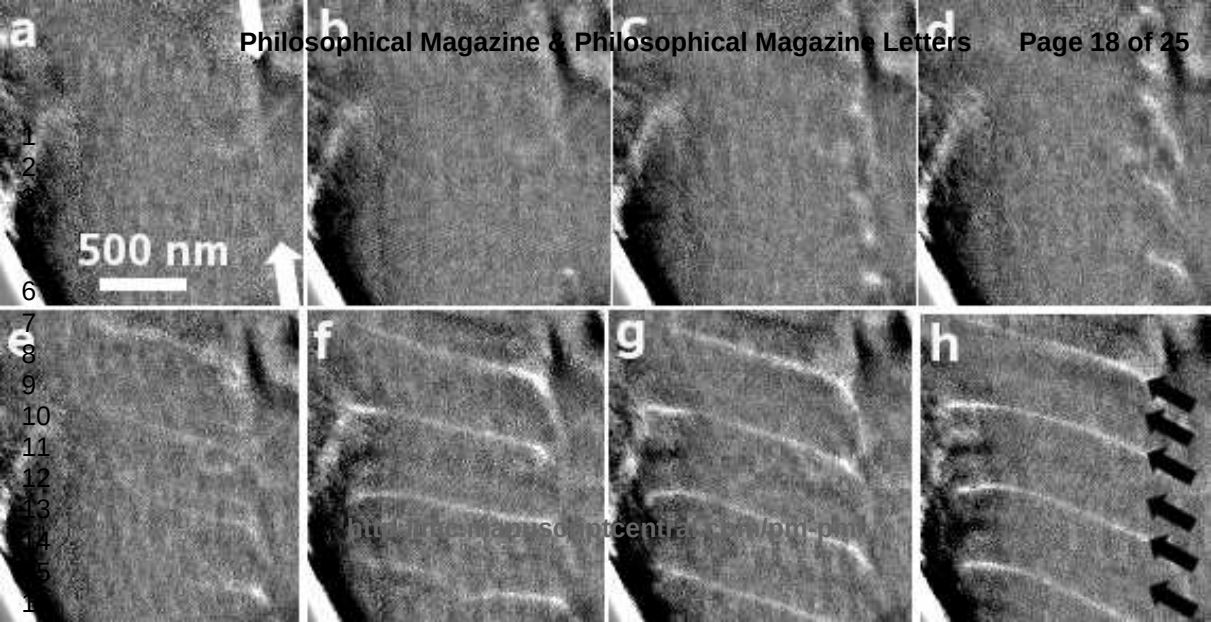

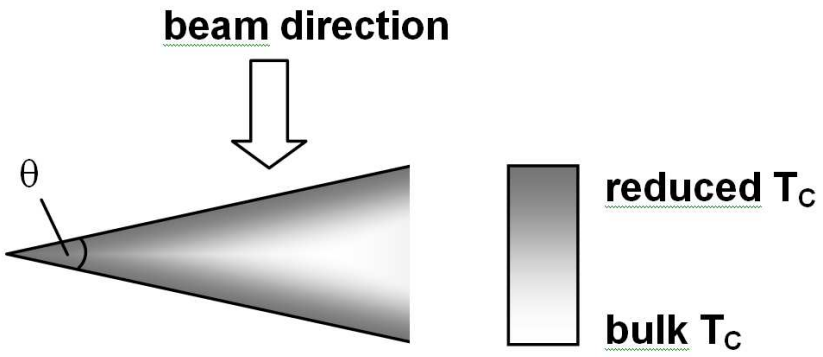

Figure 4
306x171mm (96 x 96 DPI)

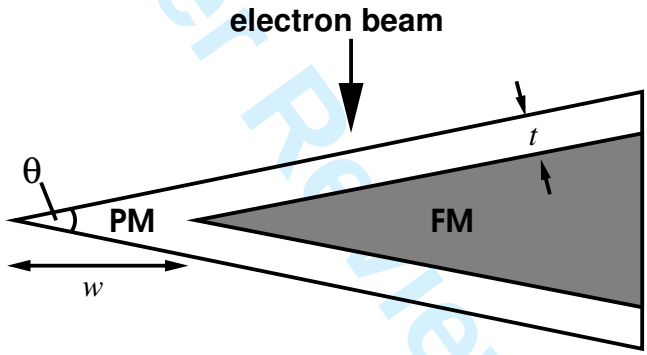

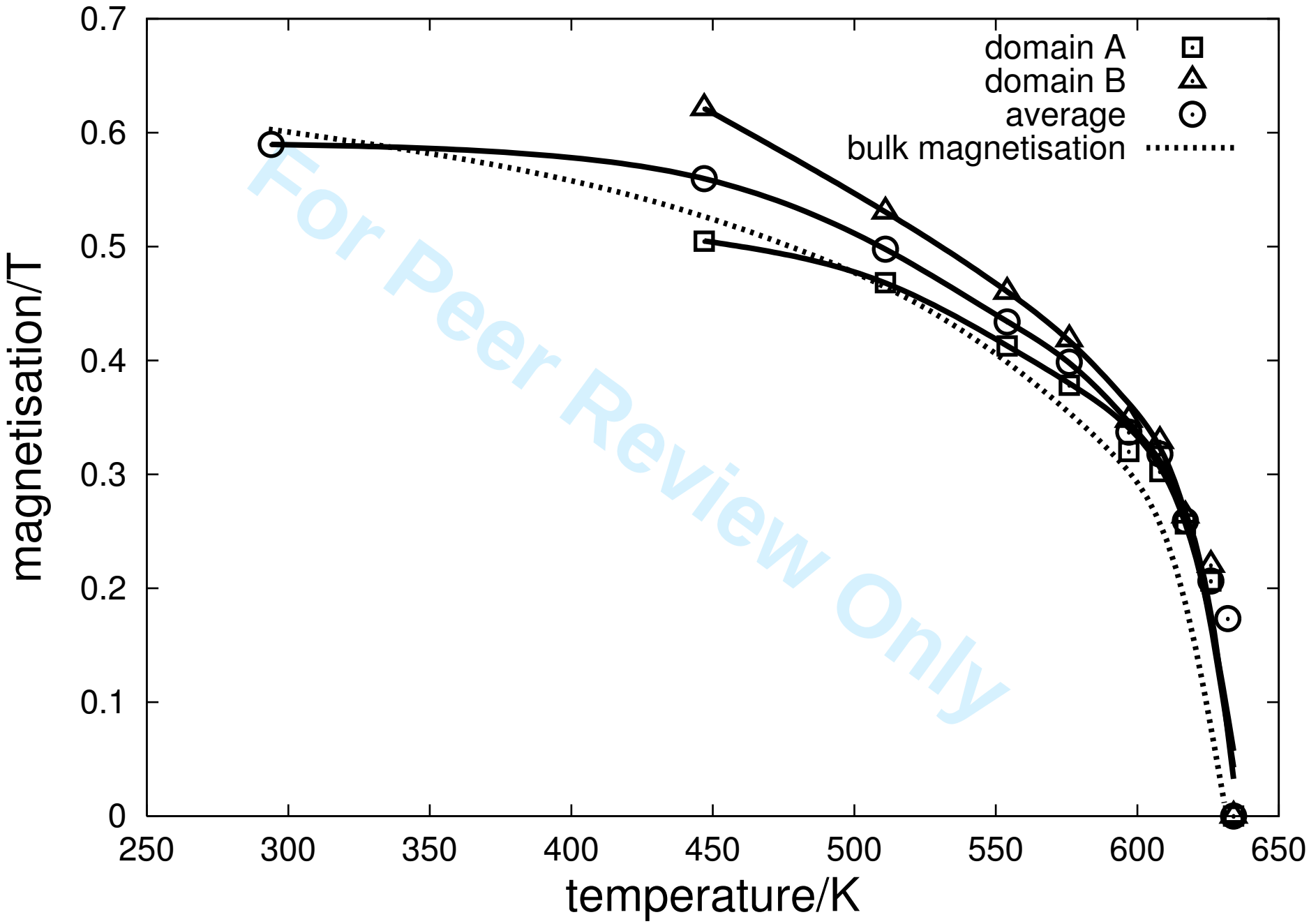

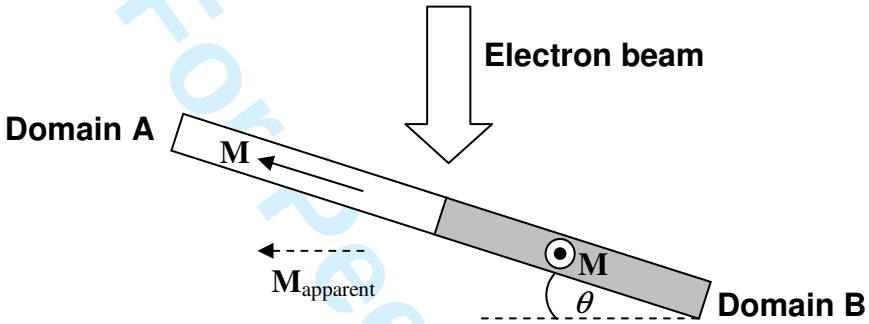

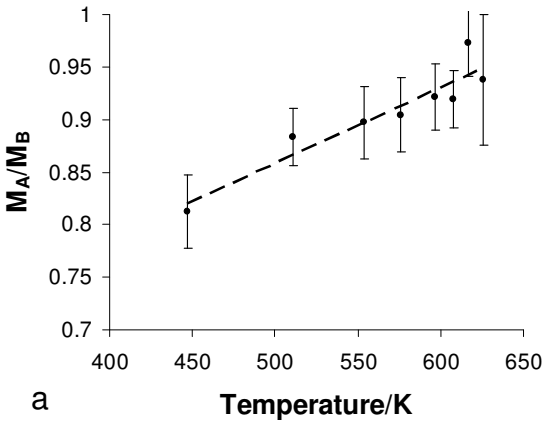

a

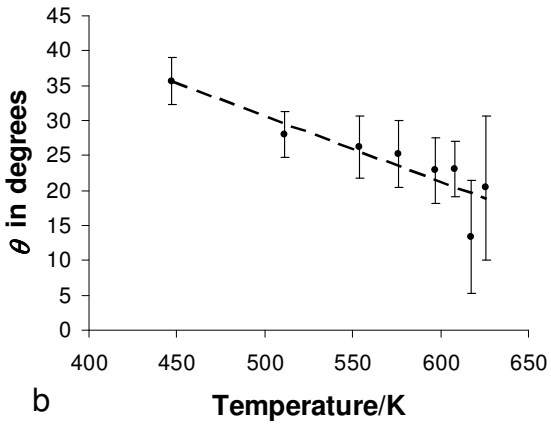

b

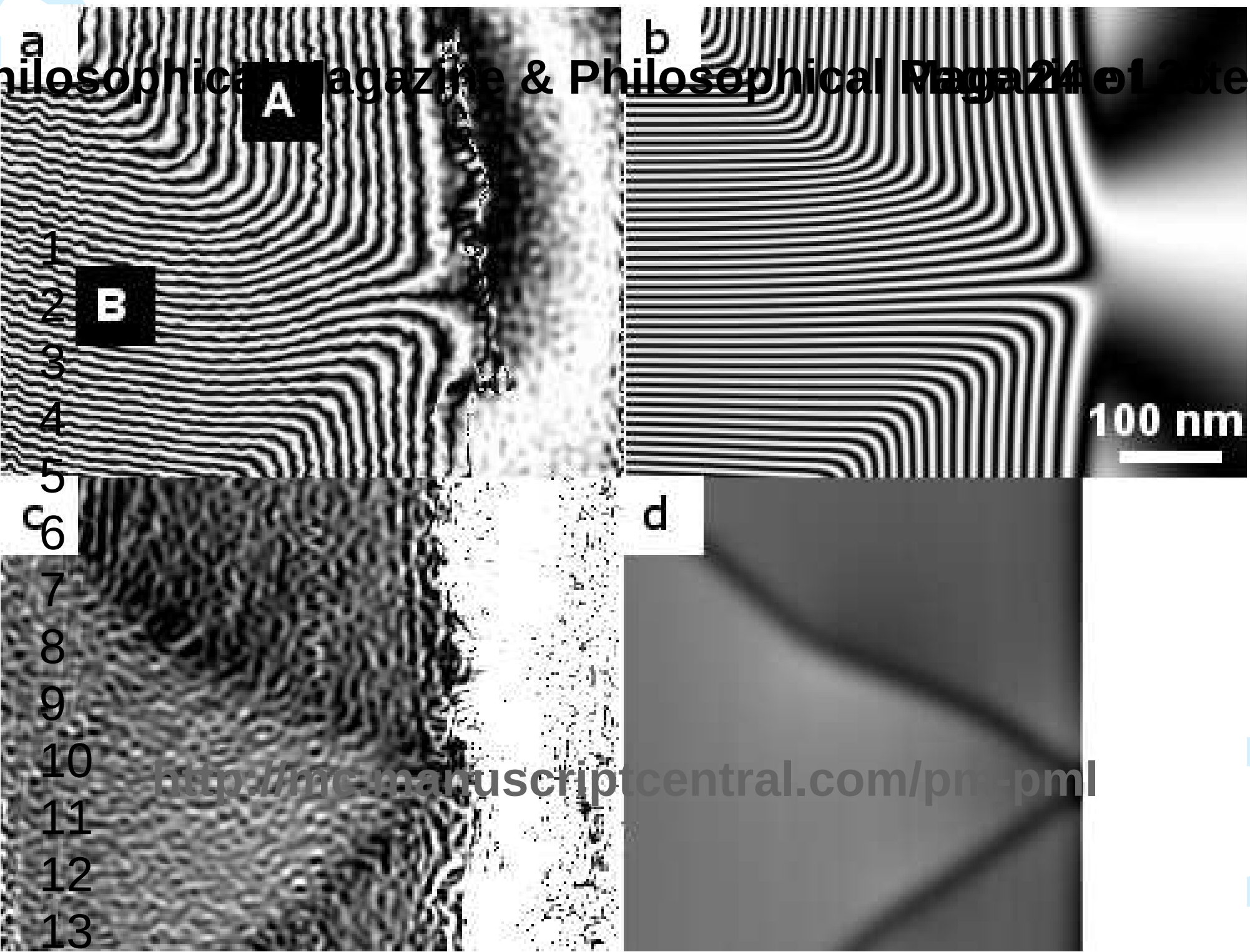

Temperature/K	w/nm	t_{PM}/nm	M*/(μ_B/Mn)	M/(μ_B/Mn)
242 ± 2	120 ± 30	16 ± 4	1.67 ± 0.04	2.1 ± 0.5
243 ± 2	180 ± 40	23 ± 6	1.46 ± 0.04	2.1 ± 0.5
244 ± 2	300 ± 70	40 ± 10	1.23 ± 0.03	2.2 ± 0.5